PHYSICAL REVIEW D **94,** 025023 (2016)

# Tunneling from a Minkowski vacuum to an AdS vacuum: A new thin-wall regime

Ali Masoumi,[1,*] Sonia Paban,[2,†] and Erick J. Weinberg[3,‡]

[1]*Institute of Cosmology, Department of Physics and Astronomy, Tufts University, Medford, Massachusetts 02155, USA*

[2]*Department of Physics and Texas Cosmology Center, The University of Texas at Austin, Austin, Texas 78712, USA*

[3]*Physics Department, Columbia University, New York, New York 10027, USA*

(Received 20 April 2016; published 14 July 2016)

Using numerical and analytic methods, we study quantum tunneling from a Minkowski false vacuum to an anti-de Sitter true vacuum. Scanning the parameter space of theories with quartic and nonpolynomial potentials, we find that for any given potential tunneling is completely quenched if gravitational effects are made sufficiently strong. For potentials where $\epsilon$, the energy density difference between the vacua, is small compared to the barrier height, this occurs in the thin-wall regime studied by Coleman and De Luccia. However, we find that other potentials, possibly with $\epsilon$ much greater than the barrier height, produce a new type of thin-wall bounce when gravitational effects become strong. We show that the critical curve that bounds the region in parameter space where the false vacuum is stable can be found by a computationally simple overshoot/undershoot argument. We discuss the treatment of boundary terms in the bounce calculation and show that, with proper regularization, one obtains an identical finite result for the tunneling exponent regardless of whether or not these are included. Finally, we briefly discuss the extension of our results to transitions between anti-de Sitter vacua.

DOI: 10.1103/PhysRevD.94.025023

## I. INTRODUCTION

The possibility of transitions between field theory vacua in curved spacetime has been a subject of considerable interest ever since the seminal paper of Coleman and De Luccia (CDL) [1] incorporated gravitational effects into the bounce formalism [2–4]. More recently the possibility of a string theory landscape has brought renewed interest in the subject.

Considerable attention has been focused on transitions between de Sitter vacua. These could well have occurred in our past. They could also be part of an eternal future, thanks in part to the fact that the thermal nature of de Sitter space allows one to tunnel upward [5] as well as downward. Somewhat less attention has been paid to transitions that end in an anti-de Sitter (AdS) vacuum. Because one cannot tunnel upward from an AdS vacuum, such transitions cannot be part of our past, but could be part of our future. If they are, it will be a grim future, because a bubble of AdS space soon develops a singularity [1,6].

However, even if there are AdS vacua, we may be protected against this fate. Working in the context of the thin-wall approximation, CDL found that gravitational effects reduce the rate for tunneling from a Minkowski vacuum to an AdS vacuum; if the difference in vacuum energy densities is sufficiently small, the decay is completely forbidden [1,7,8]. This result can be extended to transitions between AdS vacua [9]. If the initial vacuum is de Sitter, tunneling is suppressed, although complete suppression is only possible in the flat-space limit of vanishing vacuum energy density [10,11].

Decays to AdS vacua beyond the thin-wall limit were studied by Samuel and Hiscock [12] and others [13–19]. In this paper we go beyond these works by considering a wider range of potentials and parameters. By doing so we uncover some apparently universal properties of these transitions that were not previously recognized. Perhaps most notably, we find a strong gravity regime in which a new type of thin-wall bounce emerges.

We focus on transitions from a Minkowski false vacuum with vanishing cosmological constant to an AdS vacuum with negative energy density $-\epsilon$. The case where $\epsilon$ is small compared to the height $U_{\rm top}$ of the potential barrier between the false vacuum and the AdS true vacuum is amenable to the thin-wall approximation, and it was this case that was studied in detail by CDL. We will be concerned with the more general case, including theories where, at least in the absence of gravity, the transition is mediated by Euclidean solutions that are very definitely thick-wall bounces.

Although we restrict ourselves to theories with a single scalar field, we expect our results to generalize to more complex theories, including those where suppression of vacuum decay is due to supersymmetry, either exact or nearly so [20–23].

*ali@cosmos.phy.tufts.edu
†paban@zippy.ph.utexas.edu
‡ejw@phys.columbia.edu

 

In the usual, small $\epsilon$, thin-wall approximation the bounce consists of a thin spherical shell that separates an interior true vacuum region from a false vacuum exterior. If the potential is modified so that $\epsilon$ is decreased, the thickness of the shell is unchanged, while the bounce radius grows. The thin wall bounces that we find arise when the gravitational constant $\kappa = 8\pi G$ is increased while the potential $U(\phi)$ is held fixed (or, equivalently, if all mass scales in the potential are increased by a uniform factor with $\kappa$ kept constant). They consist of a spherical region of pure AdS true vacuum that is enclosed by a transition region that is composed of an inner part with a spatially varying negative energy density and an outer part where the matter field traverses the potential barrier. When $\kappa$ is increased, the field profile in the transition region and the thickness of this region (measured in an appropriate coordinate) vary only weakly, while the radius of the true vacuum region grows and becomes infinite at a potential-dependent critical value $\kappa_{\rm cr}$. The bounce action diverges as this critical value is approached, so that tunneling is completely quenched for $\kappa \geq \kappa_{\rm cr}$.

The remainder of the article is arranged as follows. In Sec. II we review the bounce formalism for vacuum decay, including the usual thin-wall approximation. We also review some energy considerations that play a role in the suppression of vacuum decay at large $\kappa$. In Sec. III we present numerical results for bounces in both quartic polynomial and nonpolynomial potentials, with a range of both the parameters in the potentials and of values of $\kappa$. In Sec. IV we analyze these numerical results and present analytic arguments that explain some of the properties that we have uncovered. Section V contains some concluding remarks. There are three appendices. Appendix A discusses possible boundary terms in bounce calculations, and shows that their inclusion or omission, if done properly, has no effect on the decay rate. Appendix B gives details of our numerical methods. Appendix C discusses the extension of our results to decays from one AdS vacuum to another.

## II. SETUP AND SUMMARY OF PREVIOUS RESULTS

### A. Basic formalism

In this paper we will be concerned with vacuum transitions in a theory with the dynamics of a scalar field $\phi$ governed by a potential such as that shown in Fig. 1. Without loss of generality we have set the true vacuum at $\phi_{\rm tv} = 0$ and put the false vacuum to its right, at $\phi_{\rm fv} \equiv v > 0$. The peak of the potential barrier separating the two vacua is at $\phi_{\rm top}$. The values of the potential at these points are $U_{\rm tv} = -\epsilon$, $U_{\rm fv} = 0$, and $U_{\rm top}$, respectively. It is important to note that $\epsilon$ is not necessarily small; indeed, we will consider some cases in which it is rather large.

An initial false vacuum state can decay by the nucleation of bubbles of true vacuum, with a nucleation rate per unit volume that can be written in the form

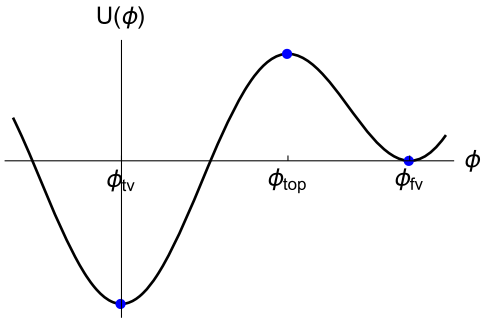


FIG. 1. A quartic potential with two minima.

$$\frac{\Gamma}{\mathcal{V}} = Ae^{-B}. \tag{2.1}$$

In the absence of gravity, this nucleation rate can be calculated with the aid of a bounce solution $\phi_b(x)$ of the Euclidean field equations that begins with a configuration of spatially homogeneous false vacuum at Euclidean time $x_4 = -\infty$, evolves to a configuration containing a true vacuum bubble at $x_4 = 0$, and then returns in an $x_4$-reversed fashion to a false vacuum configuration at $x_4 = \infty$ [2,3]. The tunneling exponent

$$B = S(\phi_b) - S(\phi_{\rm fv}) \tag{2.2}$$

is the difference between the Euclidean action of the bounce and that of the pure false vacuum.[1] The Lorentzian configuration at nucleation is given by a spacelike slice through the bounce at $x_4 = 0$; at nucleation the Lorentzian-time field is instantaneously at rest.

Coleman and De Luccia argued that the effects of gravity on bubble nucleation could be incorporated by adding a gravitational contribution to the action, which for a theory with a single scalar field then reads

$$S = \int d^4x\sqrt{g}\left[\frac{1}{2}g^{ab}\partial_a\phi\partial_b\phi + U(\phi) - \frac{1}{2\kappa}R\right] + S_{\rm bdy}. \tag{2.3}$$

Here the last term in the integral is the Einstein-Hilbert action, with $\kappa = 8\pi G_N$, while $S_{\rm bdy}$ is the Euclidean version of the Gibbons-Hawking boundary action [24].

This boundary term, which does not appear explicitly in Ref. [1], requires some comment. Decays from a de Sitter vacuum are governed by compact bounces, so there is no boundary term. On the other hand, the bounces for decays from Minkowski or anti-de Sitter vacua are infinite in extent, so their actions are potentially divergent, as are the Gibbons-Hawking terms, and must be regularized. The physically significant quantity is the difference $B$ between the actions of the bounce and of the pure false vacuum. We show in Appendix A that with proper regularization $B$ is

[1]Because all actions in this paper will be Euclidean, we will simplify notation by omitting a subscript $E$.

finite and independent of whether or not the Gibbons-Hawking term is included.

For a single scalar field, it is known that in flat spacetime the bounce has O(4) symmetry [25]. Although no comparable result has been proven for curved spacetime, in this work we will assume the same symmetry. With this symmetry the metric takes the form:

$$ds^2 = d\xi^2 + \rho(\xi)^2 d\Omega_3^2. \tag{2.4}$$

The action can then be written as

$$S = 2\pi^2 \int_{\xi_{\min}}^{\xi_{\max}} d\xi \left\{ \rho^3 \left[ \frac{1}{2}\phi'^2 + U(\phi) \right] + \frac{3}{\kappa}(\rho^2\rho'' + \rho\rho'^2 - \rho) \right\} - \frac{6\pi^2}{\kappa}\rho^2\rho' \Big|_{\xi=\xi_{\min}}^{\xi=\xi_{\max}} \tag{2.5}$$

with primes indicating differentiation with respect to $\xi$. An integration by parts, with the boundary term exactly canceled by the Gibbons-Hawking term, gives

$$S = 2\pi^2 \int_{\xi_{\min}}^{\xi_{\max}} d\xi \left\{ \rho^3 \left[ \frac{1}{2}\phi'^2 + U(\phi) \right] - \frac{3}{\kappa}(\rho\rho'^2 + \rho) \right\}. \tag{2.6}$$

The equations of motion that follow from this action are

$$\phi'' + 3\frac{\rho'}{\rho}\phi' = \frac{dU}{d\phi}, \tag{2.7}$$

$$\rho'^2 = 1 + \frac{\kappa}{3}\rho^2 \left[ \frac{1}{2}\phi'^2 - U(\phi) \right]. \tag{2.8}$$

A further useful equation, obtained by differentiating Eq. (2.8) and then using Eq. (2.7), is

$$\rho'' = -\frac{\kappa}{3}[\phi'^2 + U(\phi)]\rho. \tag{2.9}$$

The boundary conditions for these equations depend on the topology of the solution. To avoid a singularity, $\phi'$ must vanish at any zero of $\rho$. In all bounce solutions there is at least one such zero, which can be taken to lie at $\xi = 0$. Bounces describing decays from a de Sitter vacuum have a second zero (and thus an $S^4$ topology), but for decays from an anti-de Sitter or Minkowski vacuum, such as we are concerned with in this work, any acceptable bounce must have an $R^4$ topology and thus only a single zero of $\rho$. We thus have $\xi_{\min} = 0$ and $\xi_{\max} = \infty$ and the boundary conditions

$$\phi'(0) = 0, \qquad \phi(\infty) = \phi_{\rm fv}, \qquad \rho(0) = 0. \tag{2.10}$$

The field equations can be used to obtain simpler expressions for the action of the bounce solution. First, as pointed out by CDL, substitution of Eq. (2.8) into Eq. (2.6) gives

$$S = 4\pi^2 \int_0^\infty d\xi \left[ \rho^3 U(\phi) - \frac{3}{\kappa}\rho \right]. \tag{2.11}$$

Note that this integral will be divergent for both the bounce and for the initial false vacuum. An alternative expression is obtained by substituting Eqs. (2.8) and (2.9) for $\rho'^2$ and $\rho''$ into Eq. (2.5). This gives

$$S = -2\pi^2 \int_0^\infty d\xi\ \rho^3 U(\phi) + \text{boundary terms}. \tag{2.12}$$

For decay from a Minkowski vacuum the boundary terms of the bounce and of the false vacuum cancel in the calculation of $B$. Since $U(\phi)$ is identically zero in the false vacuum, we then have

$$B = -2\pi^2 \int_0^\infty d\xi\ \rho^3 U(\phi). \tag{2.13}$$

### B. Thin-wall approximation

Coleman and De Luccia computed the bounce action in the thin-wall approximation. In this limit we can easily distinguish three regions in the profile of the field $\phi$: a region of pure true vacuum (inside the bounce), a region of pure false vacuum (outside the bounce) and a well-defined thin wall at $\rho = \bar{\rho}$ separating the two regions. This approximation requires that the energy difference between the two vacua,

$$\epsilon = U(\phi_{\rm fv}) - U(\phi_{\rm tv}), \tag{2.14}$$

be small compared to the other mass scales in the potential.

The existence of these distinct regions suggests splitting the integration region in the actions into three parts, whose contributions to the tunneling exponent are

$$B_{\rm outside} = 0, \tag{2.15}$$

$$B_{\rm wall} = 2\pi^2\bar{\rho}^3\sigma \equiv 4\pi^2\bar{\rho}^3 \int d\xi [U(\phi) - U(\phi_{\rm fv})], \tag{2.16}$$

$$B_{\rm inside} = \frac{12\pi^2}{\kappa^2} \left\{ \frac{1}{U(\phi_{\rm tv})} \left[ \left( 1 - \frac{\kappa}{3}\bar{\rho}^2 U(\phi_{\rm tv}) \right)^{3/2} - 1 \right] - (\phi_{\rm tv} \to \phi_{\rm fv}) \right\}. \tag{2.17}$$

These expressions only depend on the location $\bar{\rho}$ of the wall, the values of the potential at the vacua, and the surface tension $\sigma$ of the wall. The location of the wall is determined by requiring that it be a stationary point of the action.

For transitions from Minkowski to anti-de Sitter the wall is located at

$$\bar{\rho} = \frac{\bar{\rho}_0}{1 - (\bar{\rho}_0/2\ell)^2}, \tag{2.18}$$

where $\bar{\rho}_0 = 3\sigma/\epsilon$ is the location of the wall in the absence of gravity, and

$$\ell = (\kappa\epsilon/3)^{-1/2} \tag{2.19}$$

is the anti-de Sitter radius. The tunneling exponent is

$$B = \frac{B_0}{[1 - (\bar{\rho}_0/2\ell)^2]^2}, \tag{2.20}$$

where the subscript zero indicates the value of the action in the absence of gravitational effects. If we define a critical value

$$\kappa_{\rm cr} = \frac{4\epsilon}{3\sigma^2}, \tag{2.21}$$

the above results can written as

$$\bar{\rho} = \frac{\bar{\rho}_0}{(1 - \kappa/\kappa_{\rm cr})}, \tag{2.22}$$

and

$$B = \frac{B_0}{(1 - \kappa/\kappa_{\rm cr})^2}. \tag{2.23}$$

Gravity quenches vacuum decay when $\bar{\rho}_0 \geq 2\ell$ or, equivalently, when $\kappa \geq \kappa_{\rm cr}$.

For comparison with later results, we note that the thin-wall approximation for a theory with a quartic potential with almost degenerate vacua at $\phi = 0$ and $\phi = v$ predicts that the field profile in the wall is

$$\phi = \frac{v}{2}\left\{\tanh\left[\frac{\mu}{2}(\xi - \bar{\xi})\right] + 1\right\}, \tag{2.24}$$

where $\mu^2 = U''(\phi_{\rm fv})$.

### C. Energy considerations

Quantum tunneling in Minkowski space must conserve energy. With gravitational effects ignored, this implies that the energy of the spherically symmetric and instantaneously static configuration at the time of bubble nucleation must vanish; i.e.,

$$0 = 4\pi \int dr\ r^2 \left(\frac{1}{2}\phi'^2 + U\right). \tag{2.25}$$

This constraint is modified a bit when gravity is taken into account. Recall that a static spherically symmetric metric can be written in the form

$$ds^2 = -B(r)dt^2 + A(r)dr^2 + r^2 d\Omega_2^2. \tag{2.26}$$

Einstein's equations lead to

$$A(r) = \left[1 - \frac{2G_N\mathcal{M}(r)}{r}\right]^{-1}, \tag{2.27}$$

where

$$\mathcal{M}(r) = 4\pi \int_0^r ds\ s^2\tilde{\rho}(s) \tag{2.28}$$

with $\tilde{\rho}$ the energy density. Conservation of energy becomes the requirement that the ADM mass $M = \mathcal{M}(\infty)$ vanish. For our scalar field theory,

$$\begin{aligned}\tilde{\rho} &= \frac{1}{2A}\left(\frac{d\phi}{dr}\right)^2 + U \\ &= \frac{1}{2}\left(\frac{d\phi}{d\xi}\right)^2 + U.\end{aligned} \tag{2.29}$$

If we identify $\rho$ with $r$ on the $x_4 = 0$ spacelike surface, our requirement becomes

$$\begin{aligned}0 &= 4\pi \int_0^\infty d\rho\ \rho^2 \left(\frac{1}{2}\phi'^2 + U\right) \\ &= 4\pi \int_0^\infty d\xi\ \rho^2\rho' \left(\frac{1}{2}\phi'^2 + U\right).\end{aligned} \tag{2.30}$$

Now note that

$$\begin{aligned}\frac{d}{d\xi}\left[-\rho^3\left(\frac{1}{2}\phi'^2 - U\right)\right] &= \rho^3\left(-\phi'\phi'' + \phi'\frac{dU}{d\phi}\right) \\ &\quad - 3\rho^2\rho'\left(\frac{1}{2}\phi'^2 - U\right) \\ &= 3\rho^2\rho'\left(\frac{1}{2}\phi'^2 + U\right),\end{aligned} \tag{2.31}$$

where the second equality is obtained by using Eq. (2.7) to eliminate $\phi''$. The quantity in brackets clearly vanishes at $\xi = 0$. It also vanishes as $\xi \to \infty$, provided that $\phi'^2$ and $U$ fall faster than $1/\rho^3$, which they do for a bounce describing decay from a Minkowski vacuum.

Hence, any solution of the Minkowski to AdS bounce equations is guaranteed to conserve energy. If energy cannot be conserved, then tunneling is impossible. Indeed, both CDL and S. Weinberg [20] explain the absence of tunneling when $\kappa \geq \kappa_{\rm cr}$ by showing that in this regime it is impossible to construct a thin-wall bounce that conserves energy. We will see presently how this line of argument can be applied beyond the usual thin-wall approximation.

## III. THICK-WALL BOUNCES—NUMERICAL RESULTS

The thin-wall approximation has the attractive feature of producing analytic expressions for the bounce action and for the field profile of the bounce. Unfortunately, its validity is restricted to a rather special class of potentials, those for which $\epsilon$, the difference in energy densities between the true and false vacua, is small compared to the scale set by the potential barrier separating the two vacua. It is well known that in the absence of gravity a generic potential that does not satisfy this criterion can yield a "thick-wall" bounce solution in which the scalar field, even at the center of the bounce, is never close to its true vacuum value. We have explored a number of such potentials, following the evolution of the bounce as the strength of gravity is increased. In this section we will use several examples to illustrate the generic features that we have found.

First, we consider a number of quartic potentials. An arbitrary quartic potential can be written in the form

$$U(\phi) = \lambda(C_0 + C_1\phi + C_2\phi^2 + C_3\phi^3 + \phi^4). \tag{3.1}$$

We will assume that $\lambda$ is positive and that the other coefficients are such that $U$ has two minima.

Variation of the constants gives five degrees of freedom. Two, corresponding to translations in the $U$-$\phi$ plane, are fixed by our convention that the true vacuum be at $\phi_{\rm tv} = 0$ and the requirement that $U_{\rm fv} = 0$; the former implies that $C_1 = 0$, while the latter imposes a constraint relating $\epsilon = -\lambda C_0$, $C_2$, and $C_3$.

Two more degrees of freedom correspond to rescalings of the height and width of the potential. The first of these is implemented by varying $\lambda$. At the classical level, the effects of this can be absorbed by a rescaling of the length scale. Simple scaling arguments show that the bounce action is proportional to $1/\lambda$, while the width of the field profile is proportional to $1/\sqrt{\lambda}$. In our investigation of the bounce solutions, we find it convenient to work with $\lambda = 1$, keeping in mind the possibility of restoring $\lambda$ by a rescaling. In particular, we will be led to consider solutions with fields comparable to or greater than the Planck mass. By choosing a suitably small value of $\lambda$, the energies associated with these solutions can always be made sub-Planckian.

Rescaling the width of the potential is implemented by varying the position of the false vacuum, which we denote by $\phi_{\rm fv} = v$. This leaves one remaining degree of freedom. Although this could be implemented by varying a single coefficient in the potential, we find it more instructive to parameterize it by the value of $U_{\rm top}$, a quantity that can be naturally generalized to other, nonpolynomial, potentials. In Fig. 2, we show the effects of separate variations of the dimensionless quantities $U_{\rm top}/v^4$ and $\epsilon/v^4$.

We will investigate the effects of gravity by following the evolution of the bounce solutions as the mass scales in the potential are increased. In order to separate the effects of a stronger gravitational interaction from those due to a variation of the field dynamics, we will keep the shape of the potential unchanged. Thus, we will vary $v$ but hold $\epsilon/v^4$ and $U_{\rm top}/v^4$ fixed. The quantity

$$\beta = \sqrt{\kappa v^2} = \frac{\sqrt{8\pi}\, v}{M_{\rm Pl}} \tag{3.2}$$

can then be viewed as a measure of the relative strength of the gravitational interactions. Thus $\beta$ and $U_{\rm top}/\epsilon$ can be taken as the dimensionless quantities spanning the parameter space of our potentials.

It may be helpful to relate our parameterization of the quartic potential with that used in Refs. [10] and [11]. For the case of a Minkowski false vacuum, that potential can be written as

$$U(\tilde{\phi}) = \left(\frac{\mu}{M}\right)^4 \left(-\frac{1}{2}M^2\tilde{\phi}^2 - \frac{b}{3}M\tilde{\phi}^3 + \frac{1}{4}\tilde{\phi}^4\right) + C \tag{3.3}$$

where the constant $C$ is chosen so that $U_{\rm fv} = 0$, and tildes have been inserted because their field is shifted relative to ours, with the top of the barrier lying at $\tilde{\phi} = 0$. The strength of gravity is measured by the quantity

$$\tilde{\epsilon} = \sqrt{\frac{8\pi}{3}}\frac{M}{M_{\rm Pl}} \tag{3.4}$$

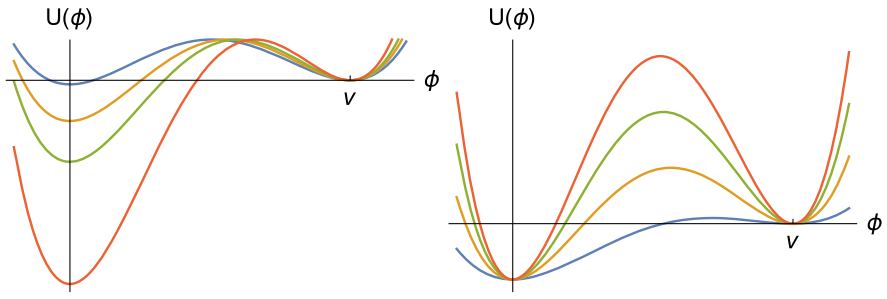


FIG. 2. Quartic potentials with fixed $U_{\rm top}$ and $\epsilon/U_{\rm top} = 0.1$, 1, 2, and 5 (on left) and fixed $\epsilon$ and $U_{\rm top}/\epsilon = 0.1$, 1, 2, and 3 (on right).

where we have inserted a tilde on their $\epsilon$ to avoid confusion with our notation for the true vacuum energy density.

Variation of their $b$ corresponds to a variation of both $\epsilon/v^4$ and $U_{\rm top}/v^4$ in our potential. When $|b|$ is small, the true and false vacuum are almost degenerate, and $U_{\rm top}/\epsilon$ is small; a large value of $|b|$ corresponds to a large $U_{\rm top}/\epsilon$. Although simple closed form expressions converting between the two sets of conventions cannot be obtained in general, matters simplify for the case $b = 1$ that was used for the numerical analysis in Refs. [10] and [11].

With $b = 1$, the true and false vacua and the top of the potential barrier occur at

$$\tilde{\phi}_{\rm tv} = \frac{1+\sqrt{5}}{2} M$$
$$\tilde{\phi}_{\rm fv} = \frac{1-\sqrt{5}}{2} M$$
$$\tilde{\phi}_{\rm top} = 0. \tag{3.5}$$

From this we find that the ratio of the barrier height to the true vacuum energy density is given by

$$\frac{U_{\rm top}}{\epsilon} = \frac{-25+13\sqrt{5}}{50} = 0.08138. \tag{3.6}$$

The distance between the minima, $v$ in our notation, is then

$$v = |\phi_{\rm fv} - \phi_{\rm tv}| = \sqrt{5} M \tag{3.7}$$

so that our measure of the strength of gravity is related to theirs by

$$\beta = \frac{\sqrt{3} v}{M} \tilde{\epsilon} = \sqrt{15}\, \tilde{\epsilon}. \tag{3.8}$$

Figures 3–5 show the evolution of the field profile with $\beta$ for several different choices of $\epsilon$ and $U_{\rm top}$. Figure 3 shows bounces for a potential with $\epsilon/U_{\rm top} = 100$. In the weak gravity limit, $\beta = 0$, the bounce is clearly a thick-wall solution, with the initial value of the field not even close to $\phi_{\rm tv}$. The corresponding bounce for a potential with $\epsilon/U_{\rm top} = 20$, shown in Fig. 4, begins closer to the true vacuum, but immediately evolves rapidly toward $\phi_{\rm fv}$; although there is a suggestion of a bubble wall, there is no clearly defined true vacuum interior. The bounces in Fig. 5 are closer to one's conception of a thin-wall bounce, but with this moderately small ratio $\epsilon/U_{\rm top} = 0.4$, the quantitative predictions of the thin-wall analysis are not borne out.

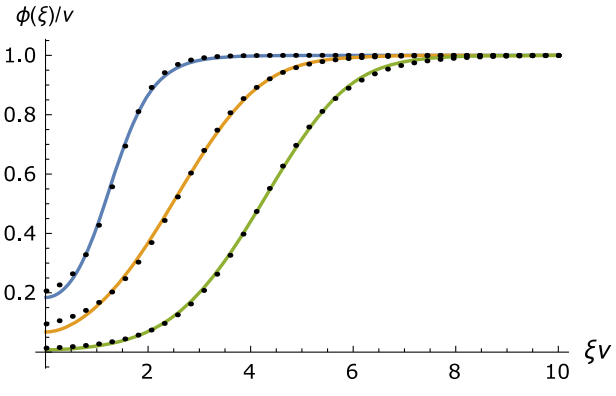


FIG. 3. Profiles of $\phi$ for the quartic potential with $U_{\rm top}/v^4 = 0.01$ and $\epsilon/v^4 = 1$. The solid curves indicate the best fit of a hyperbolic tangent to the data. Reading from left to right, the curves correspond to $\beta = 0$, 5.747, and 5.763.

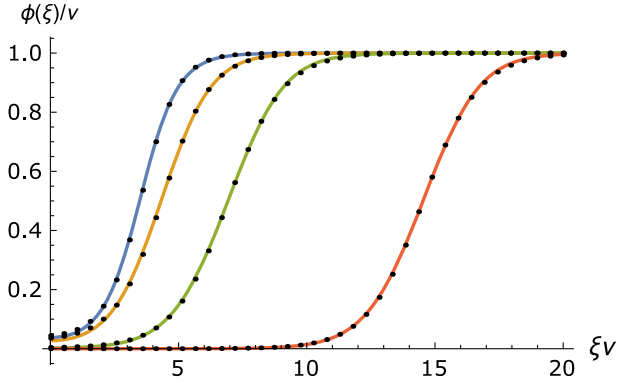


FIG. 4. Similar to Fig. 3, but for $U_{\rm top}/v^4 = 0.01$ and $\epsilon/v^4 = 0.2$. Reading from left to right, the curves correspond to $\beta = 0$, 2.70, 3.33, and 3.38.

However, in all three cases, with larger $\beta$ the transition from $\phi_{\rm tv}$ to $\phi_{\rm fv}$ occurs at larger values of $\xi$ and there is a more clearly defined transition region centered about a value $\xi = \xi_0$. As $\beta$ is increased, this transition region moves further outward, but with its shape remaining roughly constant. There is a critical value $\beta_{\rm cr}$ beyond which there is no bounce. As this value is approached, $\xi_0$ rapidly increases and, we will argue, tends to infinity in the critical limit.

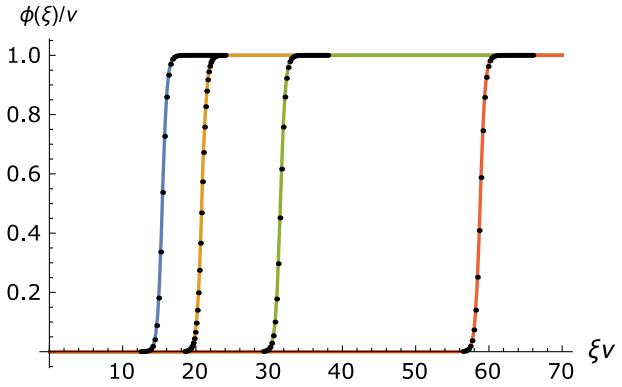


FIG. 5. Similar to Fig. 3, but for $U_{\rm top}/v^4 = 0.25$ and $\epsilon/v^4 = 0.1$. Reading from left to right, the curves correspond to $\beta = 0$, 0.588, 0.714, and 0.739.

In fact, the field profile in the transition region can be approximated by a hyperbolic tangent, with

$$\phi(\xi) \approx \frac{v}{2}\{\tanh[b(\xi - \xi_0)] + 1\}. \tag{3.9}$$

As can be seen in the figures, the fit is surprisingly good, although there is a slight mismatch where the exponential tails of the hyperbolic tangent overlap with those of the true and false vacuum regions. We do not have an analytic explanation for this behavior, which we have found in all of the examples that we have examined. As we saw in Sec. II, one also finds a hyperbolic tangent in the thin-wall approximation for a quartic potential. However, in that case the parameter $b$ could be directly read off from the potential and did not depend on $\beta$. In our more general case $b$ varies with $\beta$ (even in the quasi-thin-wall solutions of Fig. 5), decreasing as gravitational effects become stronger, and cannot be read off directly from the parameters in the potential. In the next section we will discuss the computation of $b$ in the critical limit.

There is another, quite significant difference from the thin-wall approximation. In that case, the transition region of the hyperbolic tangent clearly maps onto the potential barrier between the true and false vacua; there is no ambiguity in referring to it as the bounce wall. Matters are not so clear in the more general case. When $\epsilon$ is large compared to the height of the potential barrier, only the very last part of the transition region of the hyperbolic tangent maps onto the region where the potential is higher than in the false vacuum; i.e., onto the true barrier. The rest corresponds to an AdS-like region with a negative cosmological "constant" that decreases in magnitude as one moves outward. To emphasize this distinction, we will refer to the entire transition region as a "step," and use of the term "wall" to only refer to the region with positive potential. More specifically, we will define the wall to be the region lying between $\phi_{\rm left}$, the point on the true-vacuum side where $U(\phi) = U_{\rm fv} = 0$, and $\phi_{\rm right}$, the point on the false vacuum side where $\phi$ has gone 90% of the way from the top of the barrier to the false vacuum.

The details of the bounces for these three potentials are summarized in Tables I–III. In each table the mass scale, indicated by $\beta$, increases as one moves down the table, while the shape of the potential is held fixed. All dimensionful quantities are quoted in appropriate units of $v$ (e.g., the AdS length $\ell$ is given as a multiple of $v^{-1}$). The deviation from the true vacuum of the field at the center of the bounce is measured by the parameter

$$\eta \equiv \frac{\phi(0) - \phi_{\rm tv}}{\phi_{\rm fv} - \phi_{\rm tv}} = \frac{\phi(0)}{v}. \tag{3.10}$$

The position of the bubble wall, denoted by $\xi_{\rm wall}$ and $\rho_{\rm wall}$, is taken to be the point where $\phi = \phi_{\rm top}$, its value at the top of the barrier. The wall thickness, denoted by $\Delta\xi_{\rm wall}$ and $\Delta\rho_{\rm wall}$, is the distance between the points corresponding to $\phi_{\rm left}$ and $\phi_{\rm right}$, as defined above. The quantity $b$ is the parameter that appears in the argument of the hyperbolic tangent in Eq. (3.9). Finally, we have defined a surface tension $\sigma_{\rm wall}$ by

$$\sigma_{\rm wall} = 2\int_{\xi_{\rm left}}^{\xi_{\rm right}} d\xi[U(\phi) - U(\phi_{\rm fv})]. \tag{3.11}$$

Notice that $B$ is less than 5 for the first two entries in $\beta$ in Table I. With such small values for the

TABLE I. Data for bounces with the quartic potential, used in Fig. 3, with $U_{\rm top}/v^4 = 0.01$ and $\epsilon/v^4 = 1$ and several values of $\beta$, which is a measure of the strength of gravity. For this potential the critical value of $\beta$, at which the tunneling exponent $B$ diverges and tunneling is quenched, is $\beta_{\rm cr} = 5.7633$. The radius of the bounce wall, in coordinate and geometric units, is given by $\xi_{\rm wall}$ and $\rho_{\rm wall}$, while $\Delta\xi_{\rm wall}$ and $\rho_{\Delta\rm wall}$ give its thickness. These should be compared with the AdS length $\ell_{\rm AdS}$. The last three columns show $\eta$, a measure of how much the value of the field at the center of the bounce departs from the true vacuum value; the wall action $\sigma_{\rm wall}$; and $b$, which parameterizes the field profile in the wall. These quantities are defined more precisely in the text. All dimensionful entries are to be understood to be in units of appropriate powers of $v$.

| $\beta$ | $B$ | $\xi_{\rm wall}$ | $\rho_{\rm wall}$ | $\ell_{\rm AdS}$ | $\Delta\xi_{\rm wall}$ | $\Delta\rho_{\rm wall}$ | $\eta$ | $\sigma_{\rm wall}$ | $b$ |
|---|---|---|---|---|---|---|---|---|---|
| 0 | 4.37 | 1.92 | 1.92 | $\infty$ | 1.35 | 1.350 | 0.2181 | 0.0120 | 1.33 |
| 1.00 | 4.752 | 1.95 | 2.04 | 1.732 | 1.38 | 1.391 | 0.2247 | 0.01193 | 1.30 |
| 1.67 | 5.523 | 1.99 | 2.25 | 1.039 | 1.42 | 1.462 | 0.2349 | 0.01236 | 1.26 |
| 2.50 | 7.509 | 2.06 | 2.73 | 0.693 | 1.50 | 1.615 | 0.2499 | 0.01314 | 1.18 |
| 3.33 | 12.1 | 2.18 | 3.61 | 0.520 | 1.60 | 1.883 | 0.2622 | 0.01416 | 1.08 |
| 5.00 | 104.9 | 2.61 | 11.5 | 0.346 | 1.87 | 4.042 | 0.2442 | 0.01685 | 0.87 |
| 5.56 | 1364 | 3.05 | 42.6 | 0.312 | 1.98 | 12.13 | 0.1814 | 0.01796 | 0.77 |
| 5.71 | 25060 | 3.50 | 180 | 0.303 | 2.01 | 47.85 | 0.1171 | 0.01830 | 0.71 |
| 5.75 | $2.2 \times 10^5$ | 3.84 | 545 | 0.301 | 2.02 | 142.2 | 0.08054 | 0.01837 | 0.67 |
| 5.76 | $6.3 \times 10^6$ | 4.35 | 2918 | 0.301 | 2.03 | 756.7 | 0.04402 | 0.01840 | 0.65 |

TABLE II. The same as for Table I, but for the potential used in Fig. 4, with $U_{\rm top}/v^4 = 0.01$ and $\epsilon/v^4 = 0.2$. For this potential $\beta_{\rm cr} = 3.38058$.

| $\beta$ | $B$ | $\xi_{\rm wall}$ | $\rho_{\rm wall}$ | $\ell_{\rm AdS}$ | $\Delta\xi_{\rm wall}$ | $\Delta\rho_{\rm wall}$ | $\eta$ | $\sigma_{\rm wall}$ | $b$ |
|---|---|---|---|---|---|---|---|---|---|
| 0 | 54.2 | 4.32 | 4.318 | $\infty$ | 2.39 | 2.39 | 0.05013 | 0.0216 | 0.70 |
| 0.100 | 54.36 | 4.31 | 4.323 | 38.7 | 2.397 | 2.398 | 0.05014 | 0.0216 | 0.70 |
| 1.000 | 67.02 | 4.42 | 4.03 | 3.87 | 2.472 | 2.563 | 0.05053 | 0.0224 | 0.68 |
| 2.500 | 309.7 | 5.17 | 11.5 | 1.549 | 2.857 | 4.269 | 0.04094 | 0.0264 | 0.56 |
| 2.564 | 355.2 | 5.24 | 12.36 | 1.51 | 2.881 | 4.483 | 0.03955 | 0.0266 | 0.56 |
| 2.703 | 500.0 | 5.41 | 14.81 | 1.43 | 2.934 | 5.082 | 0.03598 | 0.0272 | 0.54 |
| 3.226 | 8678 | 6.88 | 63.9 | 1.201 | 3.165 | 16.77 | 0.01193 | 0.0295 | 0.48 |
| 3.367 | $1.1 \times 10^6$ | 9.54 | 725.2 | 1.15 | 3.236 | 173.1 | $9.9 \times 10^{-4}$ | 0.0302 | 0.46 |
| 3.378 | $4.1 \times 10^7$ | 11.6 | 4427 | 1.146 | 3.242 | 1048 | $1.3 \times 10^{-4}$ | 0.0303 | 0.46 |
| 3.380 | $1.7 \times 10^8$ | 12.4 | 9084 | 1.146 | 3.243 | 2148 | $6.0 \times 10^{-5}$ | 0.0303 | 0.46 |

TABLE III. The same as for Table I, but for the potential, used in Fig. 4, with $U_{\rm top}/v^4 = 0.25$ and $\epsilon/v^4 = 0.1$. For this potential $\beta_{\rm cr} = 0.73986$.

| $\beta$ | $B$ | $\xi_{\rm wall}$ | $\rho_{\rm wall}$ | $\ell_{\rm AdS}$ | $\Delta\xi_{\rm wall}$ | $\Delta\rho_{\rm wall}$ | $\eta$ | $\sigma_{\rm wall}$ | $b$ |
|---|---|---|---|---|---|---|---|---|---|
| 0 | 9294 | 15.5 | 15.5 | $\infty$ | 1.5 | 1.5 | $2.2 \times 10^{-19}$ | 0.36 | 1.54 |
| 0.200 | 10820 | 15.83 | 16.7 | 27.39 | 1.503 | 1.591 | $7.3 \times 10^{-20}$ | 0.37 | 1.54 |
| 0.333 | 14640 | 16.6 | 19.48 | 16.43 | 1.51 | 1.797 | $8.0 \times 10^{-21}$ | 0.37 | 1.53 |
| 0.500 | $3.2 \times 10^3$ | 18.64 | 28.73 | 10.95 | 1.525 | 2.482 | $2.1 \times 10^{-23}$ | 0.37 | 1.51 |
| 0.556 | $4.9 \times 10^4$ | 19.87 | 35.87 | 9.859 | 1.531 | 3.008 | $5.9 \times 10^{-25}$ | 0.38 | 1.51 |
| 0.588 | $6.8 \times 10^4$ | 20.85 | 42.58 | 9.311 | 1.535 | 3.503 | $3.3 \times 10^{-26}$ | 0.38 | 1.50 |
| 0.625 | $1.1 \times 10^5$ | 22.33 | 54.77 | 8.764 | 1.54 | 4.402 | $4.3 \times 10^{-28}$ | 0.38 | 1.50 |
| 0.667 | $2.6 \times 10^5$ | 24.92 | 83.49 | 8.216 | 1.546 | 6.518 | $2.1 \times 10^{-31}$ | 0.38 | 1.49 |
| 0.714 | $2.0 \times 10^6$ | 31.59 | 230.7 | 7.668 | 1.553 | 17.35 | $5.7 \times 10^{-40}$ | 0.38 | 1.48 |
| 0.735 | $6.4 \times 10^7$ | 43.67 | 1279 | 7.449 | 1.557 | 94.58 | $1.4 \times 10^{-55}$ | 0.38 | 1.48 |
| 0.739 | $1.0 \times 10^{10}$ | 58.85 | 10120 | 7.416 | 1.557 | 746.3 | $2.9 \times 10^{-75}$ | 0.38 | 1.48 |

tunneling exponent one should worry about the validity of the dilute gas approximation that underlies the bounce formalism. However, it should be kept in mind that the values in the table correspond to $\lambda = 1$; for weaker coupling $B$ would be increased by a factor of $1/\lambda$.

We have also considered a family of nonpolynomial potentials of the form

$$U = \lambda v^4 \left[ -\cos\left(\frac{\alpha\phi}{v}\right) - p\cos\left(\frac{3\alpha\phi}{v}\right) + q \right] \qquad (3.12)$$

where $\alpha$ and $q$ are determined by the requirement that there be a Minkowskian false vacuum at $\phi = v$. As with the quartic potentials, the effects of $\lambda$ at the classical level can be absorbed by a rescaling, and so for convenience we set it equal to unity. As an example, in Fig. 6 we show several bounces for a potential with $p = 0.5$, corresponding to $\epsilon/v^4 = 1.404$ and $U_{\rm top}/v^4 = 0.1925$, and give related data in Table IV.

We have observed a number of regularities that persist in all of the examples we have considered:

(1) Equations (2.22) and (2.23) show that in the thin-wall limit both the bounce radius $\bar{\rho}$ and the tunneling exponent $B$ diverge as $\kappa$ approaches a critical value, with their values being proportional to $(\kappa_{\rm cr} - \kappa)^{-1}$ and $(\kappa_{\rm cr} - \kappa)^{-2}$, respectively. Figures 7

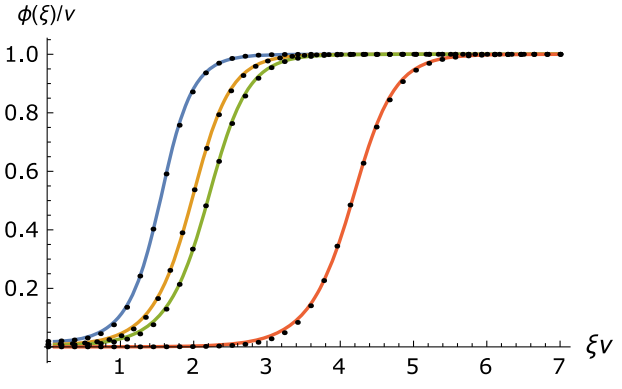


FIG. 6. Similar to Fig. 3, but for the potential of Eq. (3.12), with $p = 0.5$ and $\epsilon/U_{\rm top} = 7.30$. Reading from left to right, the curves correspond to $\beta = 0$, 2.0, 2.2 and 2.5.

TABLE IV. The same as for Table I, but for the potential used in Fig. 6. For this potential $\beta_{cr} = 2.5077$.

| $\beta$ | $B$ | $\xi_{wall}$ | $\rho_{wall}$ | $\ell_{AdS}$ | $\Delta\xi_{wall}$ | $\Delta\rho_{wall}$ | $\eta$ | $\sigma_{wall}$ | $b$ |
|---|---|---|---|---|---|---|---|---|---|
| 0 | 14.0 | 1.71 | 1.72 | $\infty$ | 1.46 | 1.5 | 0.0257 | 0.13 | 2.17 |
| 1.00 | 20.3 | 1.80 | 2.12 | 1.5 | 1.42 | 1.5 | 0.0234 | 0.14 | 2.07 |
| 2.00 | 116 | 2.18 | 5.37 | 0.73 | 1.57 | 2.3 | 0.01215 | 0.16 | 1.81 |
| 2.25 | 412 | 2.49 | 10.3 | 0.65 | 1.62 | 3.4 | $6.4 \times 10^{-3}$ | 0.16 | 1.72 |
| 2.40 | 2249 | 2.93 | 24.4 | 0.61 | 1.66 | 6.4 | $2.4 \times 10^{-3}$ | 0.17 | 1.66 |
| 2.45 | 7712 | 3.26 | 45.4 | 0.60 | 1.68 | 10.9 | $1.1 \times 10^{-3}$ | 0.17 | 1.65 |
| 2.48 | $3.3 \times 10^4$ | 3.67 | 94.2 | 0.59 | 1.68 | 21.4 | $4.1 \times 10^{-4}$ | 0.17 | 1.63 |
| 2.49 | $8.1 \times 10^4$ | 3.92 | 147 | 0.59 | 1.69 | 32.7 | $2.2 \times 10^{-4}$ | 0.17 | 1.63 |
| 2.50 | $4.2 \times 10^5$ | 4.39 | 337 | 0.58 | 1.69 | 73.3 | $6.8 \times 10^{-5}$ | 0.17 | 1.63 |
| 2.50628 | $1.2 \times 10^7$ | 5.35 | 1780 | 0.58 | 1.69 | 382 | $6.2 \times 10^{-6}$ | 0.17 | 1.63 |

and 8 illustrate similar behavior for the potentials that we have examined.

There are, however, some differences. In the thin-wall case the inverse power dependence on $(\kappa_{cr} - \kappa)^{-1}$ held for the entire range of $\kappa$. Here we see a deviation from this at small values of $\kappa$; i.e., in the parameter range where the field profile is the least "thin-wall-like." We can quantify this by comparing the the actual values of $\bar{\rho}_0$ and $B_0$ obtained from our numerical solutions with $\kappa = \beta^2 = 0$ with the values $\bar{\rho}_{fit}$ and $B_{fit}$ that would follow from extrapolating the linear behavior all the way to $\kappa = 0$. For the potentials corresponding to Tables I, II, and III, we find $B_0/B_{fit} = 0.55$, 0.77, and 0.96 and $\bar{\rho}_0/\bar{\rho}_{fit} = 0.59$, 0.76, and 0.97.

There is another difference from the thin-wall case. In that limit, $\kappa_{cr}$ corresponded to an AdS length that was exactly half the bounce radius in the absence of gravity. By contrast, the limiting value of $\ell$ for our solutions is less than half of the nongravitational bounce radius. This is consistent with the fact that the average potential in the region contained within the bounce wall is less than $\epsilon$ in magnitude, implying an effective AdS length that is larger than that of the pure true vacuum.

(2) The wall thickness as measured in $\xi$ initially increases somewhat with $\beta$, but appears to tend to a finite value in the critical limit. By contrast, the thickness as measured in $\rho$ diverges, with $\Delta\rho_{wall}/\rho_{wall}$ being roughly constant.

(3) The surface tension $\sigma_{wall}$ increases slightly with $\beta$, but tends to a finite value in the critical limit.

(4) Although $\eta$ may initially increase with $\beta$, as gravitational effects continue to grow stronger $\eta$ decreases, eventually vanishing in the critical limit.

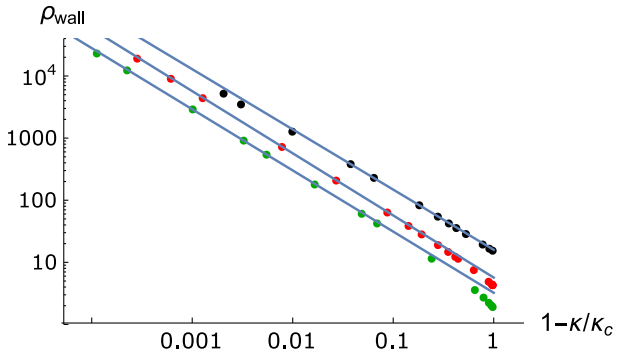


FIG. 7. The behavior of $\rho_{wall}$ (measured in units of $v^{-1}$) near the critical value of $\beta$. Reading from bottom to top, the green, red, and black circles represent the potentials for Tables I, II, and III, respectively. The best fit lines on this log-log plot have slopes −1.00, −0.99, and −0.97, respectively. Note that in each case the last three points to the right have been omitted from the fit.

## IV. ANALYTIC RESULTS

In this section we will describe how some understanding of the numerical results of the previous section can be obtained.

The plots in Figs. 3–5 show three distinct regions: Region I, $0 < \xi < \xi_1$, where the field is exponentially close to $\phi_{tv}$, Region III, $\xi_3 < \xi < \infty$, where it is exponentially close to $\phi_{fv}$, and the step, Region II, $\xi_1 < \xi < \xi_3$, that

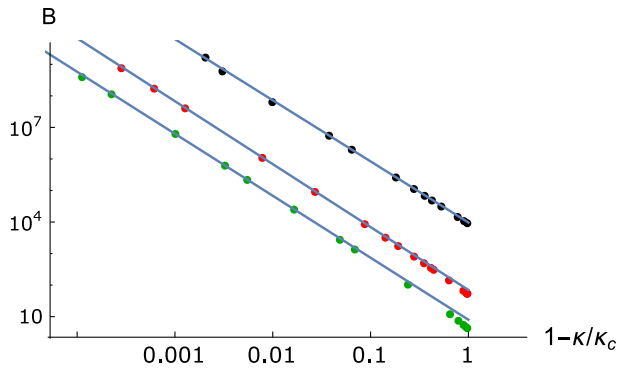


FIG. 8. Similar to Fig. 7, but for $B$. The slopes of the best fit lines are −2.00, −1.97, and −1.94.

connects the other two.[2] (As we have seen, Region I is absent for some weak gravity solutions, but it always appears once gravity is strong enough.)

In Region I $\phi$ is close to its true vacuum value, so to a good approximation Eq. (2.8) is solved by

$$\rho(\xi) = \ell \sinh(\xi/\ell). \tag{4.1}$$

In the linearized approximation Eq. (2.7) then reduces to

$$\phi'' + \frac{3\cosh(\xi/\ell)}{\ell \sinh(\xi/\ell)}\phi' = U''(\phi_{\rm tv})(\phi - \phi_{\rm tv}) \equiv \mu_t^2(\phi - \phi_{\rm tv}). \tag{4.2}$$

Changing variables to $y = \cosh(\xi/\ell)$ and setting $\phi_{\rm tv} = 0$ gives

$$(y^2 - 1)\frac{d^2\phi}{dy^2} + 4y\frac{d\phi}{dy} = \ell^2\mu_t^2\phi. \tag{4.3}$$

This has the solution

$$\phi(\xi) = \phi(0)\frac{C_\alpha^{(3/2)}[\cosh(\xi/\ell)]}{C_\alpha^{(3/2)}(1)} = \phi(0)\frac{2C_\alpha^{(3/2)}[\cosh(\xi/\ell)]}{(\alpha+2)(\alpha+1)}, \tag{4.4}$$

where $C_\alpha^{(3/2)}(y)$ is a Gegenbauer function of the first kind, with $\alpha(\alpha+3) = \mu_t^2\ell^2$. The fact that $C_\alpha^{(3/2)}(1)$ is finite for all real positive $\alpha$ guarantees that $d\phi/d\xi$ vanishes at $\xi = 0$, as required; it is this boundary condition that eliminates the Gegenbauer function of the second kind, $D_\alpha^{(3/2)}(y)$. If $\xi/\ell$ is moderately large, we can use the large argument approximation for the Gegenbauer function to obtain

$$\phi \sim e^{a\xi/\ell} \tag{4.5}$$

with

$$a = -\frac{3}{2} + \sqrt{\frac{9}{4} + \mu_t^2\ell^2}. \tag{4.6}$$

In Region III $\phi$ is close to its false vacuum value, so $\rho$ is almost linear in $\xi$, with

$$\rho(\xi) \approx \rho(\xi_3) + (\xi - \xi_3). \tag{4.7}$$

The linearized equation for $\phi$ then becomes

$$\phi'' + \frac{3}{\rho}\phi' = U''(\phi_{\rm fv})(\phi - \phi_{\rm fv}) \equiv \mu_f^2(\phi - \phi_{\rm fv}). \tag{4.8}$$

As we approach the critical solution $\rho(\xi_3)$ becomes exponentially large, so the second term in this equation can be ignored and we have

$$\phi_{\rm fv} - \phi(\xi) \sim e^{-\mu_f\xi}. \tag{4.9}$$

To understand Region II, which connects these two regions, it is helpful to follow Coleman's insight [2] and view the problem in terms of a particle moving in an upside-down potential $-U(\phi)$ while subject to a frictional force given by the $\phi'$ term in Eq. (2.7). This suggests defining a pseudo-energy

$$E = \frac{1}{2}\phi'^2 - U(\phi). \tag{4.10}$$

This is not conserved; instead, the friction term in Eq. (2.7) causes it to decrease with $\xi$, with[3]

$$E' = -3\frac{\rho'}{\rho}\phi'^2. \tag{4.11}$$

Now note that Eq. (2.8) can be recast as

$$\frac{\rho'^2}{\rho^2} = \frac{1}{\rho^2} + \frac{\kappa}{3}E. \tag{4.12}$$

For all but the very beginning of Region I, the second term dominates the right-hand side, and we can make the approximation

$$\frac{\rho'}{\rho} = \sqrt{\frac{\kappa}{3}}\sqrt{E}. \tag{4.13}$$

This continues to hold in Region II until we reach a point $\xi_2$, where $E$ has decreased enough that $(\kappa/3)E \approx 1/\rho^2$. We will refer to this interval, $\xi_1 < \xi < \xi_2$, as Region IIa. In Region IIb, $\xi_2 < \xi < \xi_3$, the first term dominates the right-hand side of Eq. (4.12). (See Fig. 9.)

In Region IIa, Eq. (4.13) leads to

$$E' = -\sqrt{3\kappa}\,\phi'^2\sqrt{E}. \tag{4.14}$$

Integrating this and noting that $E(\xi_1) \approx \epsilon$ leads to

$$\sqrt{E(\xi)} = \sqrt{\epsilon} - \sqrt{\frac{3\kappa}{4}}\int_{\xi_1}^{\xi} d\xi\,\phi'^2, \tag{4.15}$$

from which we obtain

[2]There is some freedom in defining $\xi_1$ and $\xi_3$. One could, e.g., arbitrarily choose them to be the values of $\xi$ at which $\phi$ is equal to $0.01v$ and $0.99v$.

[3]The CDL formalism allows anti-friction, with $E' > 0$; this is always encountered in decays from a de Sitter false vacuum, and might seem to be possible here when crossing the potential barrier where $U$ is positive. However, a bounce that has a period of anti-friction is necessarily compact, and therefore cannot describe decay from a Minkowski (or anti-de Sitter) vacuum.

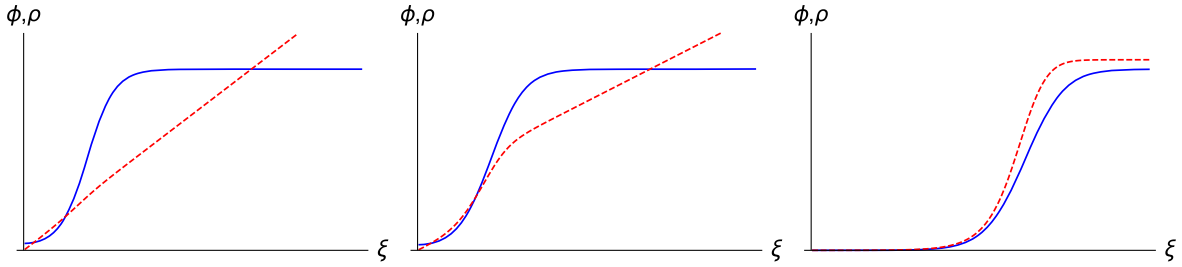


FIG. 9. The metric function $\rho$ (dashed red line) and field $\phi$ (solid blue line) in three examples with, from left to right, weak, medium, and strong gravity. The metric has been rescaled (by factors of 0.1, 0.005, and 0.00005, respectively) in order to fit it on the same graph as $\phi$. In all three cases the actual asymptotic slope of $\rho$ is unity. Note how the transition from Region IIa to Region IIb occurs later as the strength of gravity increases.

$$\rho(\xi) = \rho(\xi_1) \exp\left[\int_{\xi_1}^{\xi} d\xi \sqrt{\frac{\kappa}{3}}\sqrt{E}\right]. \tag{4.16}$$

In Region IIb (and indeed also in Region III)

$$\rho(\xi) \approx \rho(\xi_2) + (\xi - \xi_2) \tag{4.17}$$

with the linear behavior indicating that the space is approximately Minkowskian. The pseudo-energy is

$$E(\xi) = E(\xi_2) - 3\int_{\xi_2}^{\xi} d\xi \frac{1}{\rho(\xi_2) + (\xi - \xi_2)} \phi'^2. \tag{4.18}$$

As the gravitational interactions grow stronger, the transition from Region II to Region III takes place at ever larger values of $\xi_3$. In the critical limit $\xi_3 \to \infty$, the Minkowskian false vacuum is never reached and the bounce solution disappears. This limit is signaled by the vanishing of $E$ while Eq. (4.15) is still valid. This implies that

$$\int_{\xi_1}^{\infty} d\xi\ \phi'^2 = \sqrt{\frac{4\epsilon}{3\kappa}} \quad \text{(critical solution)}. \tag{4.19}$$

We can now understand why the field profile in Region II remains relatively constant for large values of $\beta$ and $\kappa$, even as the step itself moves to larger and larger $\xi$. As the critical value of $\beta$ is approached, the initial value of $\phi$ moves closer to the true vacuum, with the result that the transition from Region I to Region II occurs at a larger value of $\xi_1$. Because $\rho$ grows exponentially with $\xi$ in region I [see Eq. (4.1)], its value at the transition to Region II, $\rho(\xi_1)$, increases exponentially with increasing $\beta$.

We next note that Eq. (4.14), which governs the field profile in Region IIa, can be rewritten as

$$\phi'' + \sqrt{3\kappa}\sqrt{\frac{1}{2}\phi'^2 - U(\phi)}\ \phi' = \frac{\partial U}{\partial \phi}. \tag{4.20}$$

Because $\rho$ does not appear in this equation, the profile for $\phi$ as a function of $\xi$ does not depend on the value of $\rho$ in Region IIa. Further, Eq. (4.16) tells us that the growth factor $\rho(\xi)/\rho(\xi_1)$ is also independent of $\rho$ in this region.

Now consider Region IIb. The transition from Region IIa occurs at $\xi_2$, the point where $(\kappa/2)E = 1/\rho^2$. As $\rho(\xi_1)$ (and therefore $\rho$ throughout Region IIa) increases, this transition occurs at an ever larger value of $\xi$. This has several consequences. First, Region IIb accounts for a smaller and smaller fraction of Region II. Second, with $\rho(\xi_2)$ exponentially large in the near-critical regime, the friction term is negligible in Region IIb, implying a field profile that is independent of $\rho$. Finally, we see from Eq. (4.17) that the variation of $\rho$ in this region is negligible.

The net result is that in the near-critical regime we can write

$$\rho(\xi) = \rho(\xi_1) F(\xi - \xi_1), \tag{4.21}$$

where

$$F(\xi - \xi_1) = \exp\left[\sqrt{\frac{\kappa}{3}}\int_{\xi_1}^{\xi} d\xi\ \theta(\xi_2 - \xi)\sqrt{E}\right]. \tag{4.22}$$

In the thin-wall approximation, the absence of tunneling at large $\kappa$ could be explained by the impossibility of finding a wall radius $\bar{\rho}$ large enough that the negative contribution from the true vacuum interior exactly canceled the positive wall contribution to give zero net energy. We can now see how this generalizes to the thick wall case. Energy conservation requires that the energy integral in Eq. (2.30) vanish. The contribution to this integral from Region I is

$$\int_0^{\xi_1} d\xi\ \rho^2 \rho' U = -\frac{\epsilon}{3}\rho(\xi_1)^3, \tag{4.23}$$

up to exponentially small corrections. The contribution from Region II can be written, with the aid of Eqs. (4.13) and (4.16), as

$$\int_{\xi_1}^{\xi_2} d\xi\ \rho^3 \frac{\rho'}{\rho}\left(\frac{1}{2}\phi'^2 + U\right) = \rho(\xi_1)^3 \sqrt{\frac{\kappa}{3}}\int_{\xi_1}^{\xi_2} d\xi\ F(\xi - \xi_1)^3 \sqrt{E}\left(\frac{1}{2}\phi'^2 + U\right). \tag{4.24}$$

TABLE V. The values of $\beta_{cr}$ for the potentials considered in Tables I–IV obtained by three different methods: (i) extrapolating from the data in the tables; (ii) shooting, using Eq. (4.20); and (iii) inserting the measured value of $b$ into Eq. (4.26).

| | Extrapolation | Shooting | Using $b$ |
|---|---|---|---|
| Table I | 5.76 | 5.75 | 5.75 |
| Table II | 3.38 | 3.38 | 3.37 |
| Table III | 0.739 | 0.737 | 0.735 |
| Table IV | 2.50 | 2.50 | 2.52 |

In the strong gravity, near critical regime, Region IIa is almost all of Region II, and so the total energy is well approximated by the sum of Eqs. (4.23) and (4.24). (The contribution from Region III is exponentially small and can be neglected.)

The crucial point to note is that $\xi_1$ only enters through the factors of $\rho(\xi_1)^3$ that appear in both contributions. Because these factors are common to the contributions of Regions I and II, the flat space or weak gravity strategy of arranging a cancellation between these two by adjusting the size of the true vacuum region fails, energy cannot be conserved, and the bounce solution disappears.

We now address the determination of $\beta_{cr}$. The most obvious method for doing this is to obtain bounce equations for many values of $\beta$, look for the rapid growth in $B$ and $\rho_{wall}$ that is seen in Tables I–IV, and then extrapolate to find the value of $\beta$ where these diverge.

A second, computationally simpler, approach utilizes Eq. (4.20). A bounce solution will satisfy this equation throughout Region IIa, where the pseudo-energy term dominates Eq. (2.8), but using this equation in Region IIb would understate the friction there. A moment's thought suffices to show that if a bounce exists, then using Eq. (4.20) throughout Region II would give solutions that start at rest on the true vacuum side of the barrier and either reach or overshoot the false vacuum. In the limit of weak gravity, with $\kappa$ infinitesimal, the friction term is negligible, and conservation of pseudo-energy implies that overshooting solutions of this type will exist. On the other hand, if $\kappa$ is sufficiently large, the friction term will be strong enough to prevent $\phi$ from ever reaching the false vacuum. The critical value of $\beta$ corresponds to the boundary between these two regimes.

An even simpler method utilizes our finding that the bounce is well approximated by the hyperbolic tangent form of Eq. (3.9). Doing so and, with little error, setting the lower limit of the integral in Eq. (4.19) equal to $-\infty$, we obtain

$$\frac{1}{3}bv^2 = \sqrt{\frac{4\epsilon}{3\kappa_{cr}}} \tag{4.25}$$

or

$$\beta_{cr} = \frac{\sqrt{12\epsilon}}{bv}. \tag{4.26}$$

The data in Table V show that the three methods of determining the critical value of $\beta$ are in good agreement.

## V. CONCLUDING REMARKS

In this work we have revisited quantum tunneling from a Minkowski false vacuum to an anti-de Sitter true vacuum. We have examined polynomial and nonpolynomial potentials and scanned their parameter spaces. We have found, through a combination of analytical and numerical methods, that there is always a region of parameter space in which tunneling is quenched by gravity; i.e., for any given potential, increasing the effects of gravity by uniformly raising the mass scales in that potential will eventually render the false vacuum stable. This confirms and extends previous work [10–12].

As discussed in Sec. III, the relevant parameter space for our potentials can be spanned by two dimensionless couplings, $\beta$ and $U_{top}/\epsilon$. The former is the distance in field space between the true and false vacua divided by the Planck mass, while the latter is the ratio of the barrier height to the depth of the true vacuum. Figure 10 shows the critical line that separates the region where the false vacuum is stable against decay by bubble nucleation from the region where nucleation is possible. To determine this line it is not necessary to solve the coupled equations for $\phi$ and $\rho$. Instead, $\beta_{cr}$ can be obtained by the computationally simpler overshoot/undershoot analysis of Eq. (4.20) described in Sec. IV.

As an aside, we recall from Eq. (3.6) that that the numerical analysis of Ref. [11] corresponded to a value $U_{top}/\epsilon = 0.8138$. Our shooting method then gives $\beta_{cr} = 2.846$, and hence $\tilde{\epsilon} = 0.7346$, consistent with their result $\tilde{\epsilon} \approx 0.74$.

Figure 10 shows the critical curves for several different families of potentials. The black curve, corresponding to

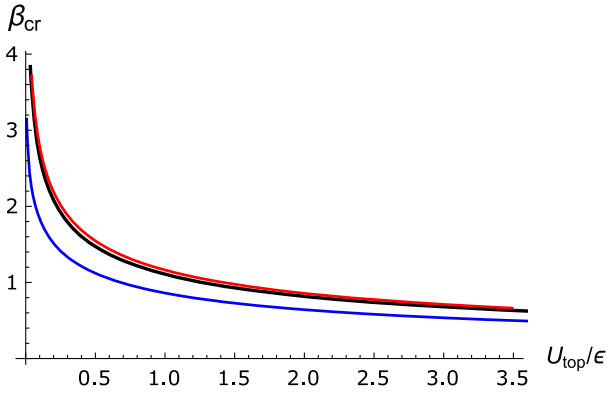


FIG. 10. Boundary of the stability region. Decay from the Minkowski false vacuum is completely quenched in the region of parameters space above and to the right of the curves. The black curve corresponds to the quartic potential, the red curve just barely above it to the nonpolynomial potentials of Eq. (3.12), and the blue to a family of potentials such as that in Fig. 11.

our quartic potentials, and the red curve, for the non-polynomial potentials of Eq. (3.12), differ very slightly in the transition region, but have the same asymptotic behaviors. The blue curve corresponds to a family of potentials of the form shown in Fig. 11. For all three cases the portion of the critical line extending to the right, at large values of $U_{\rm top}/\epsilon$, agrees well with the thin-wall approximation of CDL which predicts a power law behavior $\beta_{\rm cr} \sim (U_{\rm top}/\epsilon)^{-1/2}$. However, at smaller values of $U_{\rm top}/\epsilon$ the curves bend upward, revealing a region where tunneling is possible. The continuations of the curves upwards to large values of $\beta$ can also be fit by power laws. For the black and red curves the power is $-0.33$, while for the blue curve the power is $-0.17$, a value that varies as the width of the two wells is changed.

We expect the behavior displayed by these curves to emerge for all classes of potentials. The portion of the curve to the lower right, where $\epsilon$ is small compared to the potential barrier, corresponds to the familiar thin-wall bounces of CDL. The portion on the upper left, where the barrier becomes small, corresponds to a new type of thin-wall bounce. These evolve from thick-wall bounces as $\beta_{\rm cr}$ is approached. They are identical to the CDL-type inside and outside, but differ in the structure of the shell that separates these two regions. For the new bounces, the spherical region of AdS vacuum is enclosed by a transition region composed of an inner shell with a spatially varying negative energy density and an outer shell where the matter field transverses the energy barrier. As $\beta$ is increased the field profile and the thickness of this region (measured in the appropriate coordinate) change little while the radius of the true vacuum region increases and becomes infinite at $\beta_{\rm cr}$. These results can be generalized to the case of transitions where the initial false vacuum is AdS.

The explanation of quenching in this new class of thin-wall bounces is similar to that for the more familiar CDL class. Tunneling is only possible if an energy-conserving bubble configuration can be constructed. In flat spacetime this can always be done by making the bubble radius large enough that the negative volume energy compensates for the positive tension in the bubble wall. Because of the peculiar geometry of anti-de Sitter spacetime, this strategy begins to fail as the bubble radius approaches the AdS length $\lambda$. This can occur if a small $\epsilon$ makes the bubble large even in the absence of gravity, but it can also happen if strong gravitational effects reduce $\lambda$ relative to the length scales in the potential.

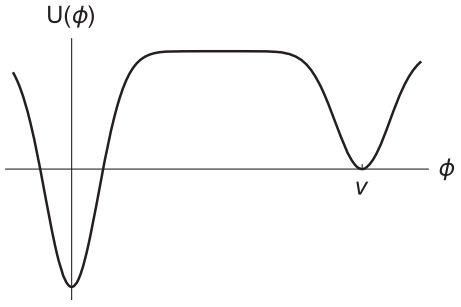


FIG. 11. One of the family of potentials, with two Gaussian potential wells, that corresponds to the blue line in Fig. 10.

The results displayed in Fig. 10 imply that for a given potential there is a set of parameters for which there are stable Minkowski vacua and, by continuation, very long-lived de Sitter vacua [10,11]. We could be living in such a vacuum, but our universe could instead be in a vacuum lying below the critical line if that its bubble nucleation rate were sufficiently small; i.e., if the tunneling exponent were sufficiently large. The minimum acceptable value of $B$ depends on the value of the dimensionful prefactor $A$ in Eq. (2.1). If $A \sim M_{\rm Pl}^4$, then our universe could have survived $\sim 10^{10}$ years if $B \gtrsim 600$; smaller values of $A$ would give smaller bounds on $B$. When comparing these bounds to the data in our tables, it should be kept in mind that the overall coupling $\lambda$ multiplies the tabulated value of $B$ by $1/\lambda$.

In the literature one finds forms for the bounce action that differ in the boundary terms. This is not an issue for transitions from a de Sitter vacuum, because these are governed by compact bounces. However, this is not the case for decays from a Minkowski or anti-de Sitter vacuum, where the corresponding bounces are noncompact. It is shown in Appendix A that with proper regularization the tunneling exponent $B$ is finite and independent of whether or not the Gibbons-Hawking boundary term is included.

Lastly, while supersymmetry, either exact or nearly so, is known to suppress tunneling [20,23], the quenching phenomenon occurs more generally; indeed, the specific potentials we have considered are not supersymmetric. It would be instructive to apply the approach of this work to the special case of almost supersymmetric theories in order to examine more closely the approach to exact supersymmetry, and thus stability, and to understand how our results generalize to theories with more fields and noncanonical kinetic terms.

## ACKNOWLEDGMENTS

We are grateful to Ken Olum for helpful discussions and advice. S. P. thanks the Institute for Advanced Study for hospitality and support during spring 2015 when this work was started. She and E. W. are grateful for the hospitality of the Aspen Center for Physics, which is supported in part by the U.S. National Science Foundation under Grant No. PHYS-1066293. This work was also supported in part by the U.S. Department of Energy under Grant No. DE-SC0011941, by the National Science Foundation under Grants No. PHY-1213888, No. PHY-1521186, and No. PHY-1316033, and by a grant from the Simons Foundation (No. 305975 to S. P.).

## APPENDIX A: BOUNDARY TERMS IN THE BOUNCE ACTION

In many discussions of vacuum decay, including the original CDL paper, the Gibbons-Hawking boundary term is omitted from the action. In this appendix we show that while the inclusion or omission of this boundary term changes the actions of the bounce and of the initial false vacuum, the tunneling exponent $B$, given by the difference between these two actions, is unchanged. We also show that, although the individual actions may be divergent, proper regularization gives a finite result for $B$ in both cases. We will assume O(4) symmetry from the start.

We define two actions by

$$S^{(1)} = 2\pi^2 \int d\xi \left[\rho^3\left(\frac{1}{2}\phi'^2 + U\right) + \frac{3}{\kappa}(\rho^2\rho'' + \rho\rho'^2 - \rho)\right] = -2\pi^2 \int d\xi\, \rho^3 U \tag{A1}$$

and

$$S^{(2)} = 2\pi^2 \int d\xi \left[\rho^3\left(\frac{1}{2}\phi'^2 + U\right) - \frac{3}{\kappa}(\rho\rho'^2 + \rho)\right] = 4\pi^2 \int d\xi \left(\rho^3 U - \frac{3}{\kappa}\rho\right). \tag{A2}$$

In each case, the second equality holds for solutions of the field equations, but not in general. The difference between the two is

$$S^{(2)} - S^{(1)} = -\frac{6\pi^2}{\kappa}\int d\xi \frac{d}{d\xi}(\rho^2\rho'). \tag{A3}$$

This is in fact equal to the Gibbons-Hawking boundary term, so $S^{(2)}$ corresponds to the action as written in Eq. (2.3).

For decay from a de Sitter vacuum, the bounce and the pure original vacuum solutions are both compact and have no boundary term, so $S^{(1)} - S^{(2)}$ clearly vanishes. We can therefore restrict our discussion to decay from a Minkowski or AdS false vacuum. In both of these cases the integrations extend out to $\xi = \infty$, and so may be infinite. To regulate these, we define $S^{(a)}(\bar{\rho})$ to be the result of integrating only from $\xi = 0$ to $\xi = \bar{\xi}$, where the latter is defined by $\rho(\bar{\xi}) = \bar{\rho}$. We then define the tunneling exponent by

$$B^{(a)} = \lim_{\bar{\rho}\to\infty} B^{(a)}(\bar{\rho}) \equiv \lim_{\bar{\rho}\to\infty}[S^{(a)}_{\rm bounce}(\bar{\rho}) - S^{(a)}_{\rm fv}(\bar{\rho})]. \tag{A4}$$

We will show that this is finite for both values of $a$. Furthermore, we will show that that $B^{(1)}$ and $B^{(2)}$ are in fact equal or, equivalently, that

$$\lim_{\bar{\rho}\to\infty} \bar{\rho}^2[\rho'_{\rm bounce}(\bar{\xi}) - \rho'_{\rm fv}(\bar{\xi})] = 0. \tag{A5}$$

### 1. Minkowski false vacuum

The pure false vacuum has $U = 0$ and $\rho = \xi$. It follows that $S^{(1)}_{\rm fv}(\bar{\rho}) = 0$ and

$$S^{(2)}_{\rm fv}(\bar{\rho}) = -\frac{6\pi^2}{\kappa}\bar{\rho}^2. \tag{A6}$$

In the bounce solution at large $\xi$, $\phi$ approaches its false vacuum value exponentially rapidly, so $U$ and $\phi'$ are both exponentially small. It then follows that $\rho'$ differs from unity by an exponentially small amount. Hence, if $\xi_1$ is well outside the bounce, then for $\bar{\xi} > \xi_1$ we have

$$\bar{\rho} = \rho(\bar{\xi}) = \rho(\xi_1) + \bar{\xi} - \xi_1 + \cdots, \tag{A7}$$

where the ellipsis represents exponentially small terms. It is then straightforward to show both that $B^{(1)}(\infty)$ is finite and that Eq. (A5) is satisfied.

### 2. AdS false vacuum

For the AdS case, let us define $\Lambda = -U_{\rm fv}$ and an AdS length

$$L = \sqrt{\frac{3}{\kappa|U_{\rm fv}|}} = \sqrt{\frac{3}{\Lambda\kappa}}. \tag{A8}$$

The pure false vacuum solution is given by $\phi = \phi_{\rm fv}$ and

$$\rho(\xi) = L\sinh(\xi/L). \tag{A9}$$

It follows that

$$S^{(1)}_{\rm fv}(\bar{\rho}) = 2\pi^2\Lambda\int_0^{\bar{\xi}} d\xi\, \rho^3 = 2\pi^2\Lambda L^4\left[\frac{1}{3}\cosh^3(\bar{\xi}/L) - \cosh(\bar{\xi}/L) + \frac{2}{3}\right]. \tag{A10}$$

At large distances the bounce solution can be written as

$$\phi(\xi) = \phi_{\rm fv} + \delta\phi(\xi), \qquad \rho(\xi) = L\sinh(\xi/L + \Delta) + \delta\rho(\xi). \tag{A11}$$

It is convenient to define $\eta = \xi/L + \Delta$. Then, to first order in $\delta\phi$, Eq. (2.7) becomes

$$\frac{d^2\delta\phi}{d\eta^2} + 3\coth\eta\frac{d\delta\phi}{d\eta} = C\delta\phi, \tag{A12}$$

where

$$C = L^2 U''(\phi_{\rm fv}). \tag{A13}$$

For $\xi \gg L$ we have

$$\frac{d^2\delta\phi}{d\eta^2} + 3\frac{d\delta\phi}{d\eta} = C\delta\phi. \tag{A14}$$

The solution with $\delta\phi$ tending to zero as $\xi \to \infty$ is

$$\delta\phi = Qe^{-a\eta}, \tag{A15}$$

where

$$a = \frac{3}{2}\left(1 + \sqrt{1 + \frac{4C}{9}}\right). \tag{A16}$$

We can now investigate the convergence of the actions. With $\xi_1 \gg L$ well outside the bounce, and $\bar\rho > \rho_1$, we have

$$\begin{aligned} B^{(1)}(\bar\rho) &= B^{(1)}(\rho_1) - 2\pi^2 \int_{\xi_1}^{\bar\xi} d\xi\, \rho^3 [U(\phi) - U_{\rm fv}] \\ &= B^{(1)}(\rho_1) - 2\pi^2 \int_{\rho_1}^{\bar\rho} d\rho \frac{\rho^3}{\rho'} [U(\phi) - U_{\rm fv}] \\ &\approx B^{(1)}(\rho_1) - \pi^2 C L^{-1} \int_{\rho_1}^{\bar\rho} d\rho\, \rho^2 \delta\phi^2. \end{aligned} \tag{A17}$$

For $\xi$ sufficiently large, $\rho \sim e^\eta$, so, using Eq. (A15), we see that $\delta\phi \sim \rho^{-a}$ and the integrand behaves as

$$\rho^{2-2a} = \rho^{-1-3\sqrt{1+4C/9}}. \tag{A18}$$

This falloff is fast enough to make the integral converge as $\bar\rho \to \infty$.

To verify that both actions lead to the same tunneling exponent, we first note that Eq. (2.8) gives

$$\rho' = \left[1 + \frac{\kappa}{3}\rho^2\left(\frac{1}{2}\phi'^2 - U\right)\right]^{1/2}. \tag{A19}$$

For $\bar\rho \gg L$ and in the asymptotic region,

$$\begin{aligned} \rho'_{\rm bounce} &\approx \frac{\rho}{L}\left\{1 + \frac{1}{2}\frac{[\delta\phi'^2 - U''(\phi_{\rm fv})\delta\phi^2]}{U_{\rm fv}}\right\}^{1/2} \\ &\approx \rho'_{\rm fv} + \frac{\rho}{4LU_{\rm fv}}[\delta\phi'^2 - U''(\phi_{\rm fv})\delta\phi^2]. \end{aligned} \tag{A20}$$

It follows that the surface term from Eq. (A5) behaves as

$$\bar\rho^2[\rho'_{\rm bounce}(\bar\xi) - \rho'_{\rm fv}(\bar\xi)] \sim \bar\rho^{3-2a}. \tag{A21}$$

Because $a > \frac{3}{2}$, this vanishes in the limit $\bar\rho \to \infty$, as required.

## APPENDIX B: NUMERICAL METHODS

In this appendix we describe the numerical techniques that we used for the calculation of the bounce and its action. The presence of very small numbers causes some complications which we address here.

Our task was to solve Eqs. (2.7) and (2.8), subject to the boundary conditions of Eq. (2.10). This can be done by a shooting code in *Mathematica*. Given the initial values $\phi'(0) = 0$ and $\rho(0)$, we choose a value for $\phi(0)$ and integrate forward until one of the following conditions is met:

(1) $\phi$ passes the false vacuum. This is an overshoot trajectory.
(2) $\phi'$ vanishes before $\phi_{\rm fv}$ has been reached. This is an undershoot trajectory.
(3) $\rho'$ vanishes. If this occurs, $\rho$ will start to decrease and eventually reach a second zero, giving a compact solution. This is unacceptable because decay from Minkowski space requires a bounce with infinite $R^4$ topology. Because $\rho'$ can only vanish when $U(\phi)$ is positive (i.e., in the potential barrier before $\phi_{\rm fv}$), this should be viewed as a undershoot trajectory.

The desired bounce solution lies at the boundary between the overshoot and undershoot regions, and can be found by bracketing this point with successive trial values of $\phi(0)$.

However, subtleties can arise. In principle, the procedure described above should work for finding all CDL solutions. However, it is not uncommon for $\phi_0$ to be exponentially close to the true vacuum. If the wall is at $\xi_{\rm wall}$, the value of $\phi_0 - \phi_{\rm tv}$ is typically of order of $e^{-m\xi_{\rm wall}}$, where $m$ is a characteristic mass scale of the problem, and $m\xi_{\rm wall}$ can be large. Therefore, we cannot represent these numbers in a machine with enough precision. However, this smallness paves the way for an analytic approximation.

We saw in Sec. IV that linearizing about the true vacuum led to the approximate solution

$$\phi(\xi) = \frac{2\phi_0 C_\alpha^{(3/2)}(\cosh\xi/\ell)}{(\alpha+2)(\alpha+1)}. \tag{B1}$$

Differentiating with respect to $\xi$ gives

$$\phi'(\xi) = \frac{3\sinh(\xi/\ell)C_{\alpha-1}^{(5/2)}[\cosh(\xi/\ell)]}{\ell C_\alpha^{(5/2)}[\cosh(\xi/\ell)]}\phi(\xi). \tag{B2}$$

If the value of $\phi(0)$ is too small, we do not integrate from $\xi = 0$. Instead we choose a value $\bar\xi$ such that the corresponding field $\phi(\bar\xi)$ from (B1) is small enough that the linearized approximation is still valid but not too small for the machine precision. We then take $\phi'(\bar\xi)$ and $\rho(\bar\xi)$ from equations Eq. (B2) and Eq. (4.1) and numerically integrate the equations of motion with these initial conditions.

TABLE VI. Similar to Table I, but for an AdS to AdS decay with $U_{\rm fv}/v^4 = -0.01$, $U_{\rm tv}/v^4 = -0.1$, and $U_{\rm top}/v = -0.005$. For this potential $\beta_{\rm cr} = 1.7502$.

| $\beta$ | $S$ | $\xi_{\rm wall}$ | $\rho_{\rm wall}$ | $\ell_{\rm AdS}$ | $\Delta\xi_{\rm wall}$ | $\Delta\rho_{\rm wall}$ | $\eta$ | $\sigma_{\rm wall}$ | $b$ |
|---|---|---|---|---|---|---|---|---|---|
| 0 | 129 | 6.47 | 6.47 | $\infty$ | 3.51 | 3.51 | 0.0432 | 0.0159 | 0.478 |
| 1.0000 | 194 | 6.93 | 8.07 | 5.48 | 3.57 | 4.22 | 0.0320 | 0.0163 | 0.462 |
| 1.5000 | 457 | 8.09 | 13.2 | 3.65 | 3.63 | 6.61 | 0.0133 | 0.0167 | 0.441 |
| 1.7000 | 1511 | 10.2 | 28.9 | 3.22 | 3.67 | 14.2 | $2.19 \times 10^{-3}$ | 0.0169 | 0.431 |
| 1.7300 | 2758 | 11.6 | 45.5 | 3.17 | 3.67 | 22.3 | $6.84 \times 10^{-4}$ | 0.0169 | 0.429 |
| 1.7450 | 6269 | 13.7 | 90.2 | 3.14 | 3.67 | 44.1 | $1.10 \times 10^{-4}$ | 0.0169 | 0.429 |
| 1.7490 | $1.46 \times 10^4$ | 16.0 | 194 | 3.13 | 3.67 | 94.6 | $1.36 \times 10^{-5}$ | 0.0169 | 0.428 |
| 1.7496 | $2.20 \times 10^4$ | 17.3 | 286 | 3.13 | 3.67 | 139 | $4.65 \times 10^{-6}$ | 0.0169 | 0.428 |
| 1.7498 | $2.86 \times 10^4$ | 18.1 | 368 | 3.13 | 3.67 | 179 | $2.33 \times 10^{-6}$ | 0.0169 | 0.428 |
| 1.7500 | $4.92 \times 10^4$ | 19.7 | 623 | 3.13 | 3.67 | 304 | $5.44 \times 10^{-7}$ | 0.0169 | 0.428 |
| 1.7501 | $1.96 \times 10^5$ | 24.0 | 2439 | 3.13 | 3.67 | 1191 | $1.26 \times 10^{-8}$ | 0.0169 | 0.428 |

## APPENDIX C: DECAYS FROM ADS VACUA

Our analysis can be easily extended to the case where both the true and the false vacua are AdS spaces. As a result, the pseudo-energy is everywhere positive definite and, except in the extremely weak gravity limit, $\rho$ is an exponentially growing function of $\xi$ throughout the transition region connecting the vacua. The second term dominates the right-hand side of Eq. (4.12) throughout Region II. We can then make the approximation

$$\frac{\rho'}{\rho} = \sqrt{\frac{\kappa}{3}\left(\frac{1}{2}\phi'^2 - U\right)}. \tag{C1}$$

This again yields Eq. (4.20) for the scalar field, and our shooting method for finding the critical value of gravity remains valid.

Data for an AdS to AdS decay are shown in Table VI. We again find complete agreement between our simulation and the critical value of $\beta$ obtained by shooting.

The behavior of the action and the wall radius as $\beta$ and $\kappa$ approach their critical values is shown in Figs. 12 and 13. Near the critical values these are fit well by

$$\bar{\rho} \sim (\kappa_{\rm cr} - \kappa)^{-1/2}, \qquad B \sim (\kappa_{\rm cr} - \kappa)^{-1/2}. \tag{C2}$$

This is in stark contrast with the decays from the Minkowski vacuum, where $B \sim (\kappa_{\rm cr} - \kappa)^{-2}$ and $\bar{\rho} \sim (\kappa_{\rm cr} - \kappa)^{-1}$. This can be understood by examining Parke's thin-wall results for an arbitrary false vacuum [9]. If the false vacuum is Minkowski, the thin-wall analysis gives an exact power law, with exponents $-2$ and $-1$, for all values of $\epsilon$. If the false vacuum is AdS, there is approximate power law behavior, with exponents $-1/2$ for both quantities, that is valid near the critical point. The region where this approximation is valid shrinks to zero as the false vacuum energy density approaches zero.

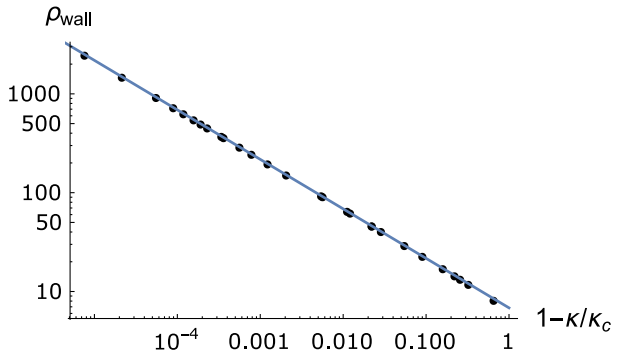


FIG. 12. Behavior of $\rho_{\rm wall}$ (measured in units of $v^{-1}$) for the potential corresponding to the data in Table VI.

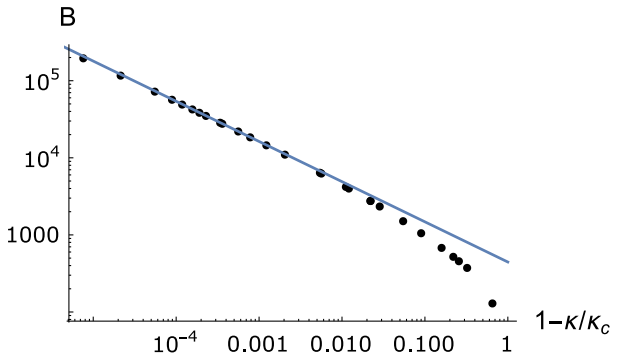


FIG. 13. Behavior of $B$ for the potential corresponding to the data in Table VI.

[1] S. Coleman and F. De Luccia, Gravitational effects on and of vacuum decay, Phys. Rev. D **21**, 3305 (1980).
[2] S. Coleman, The fate of the false vacuum. 1. Semiclassical theory, Phys. Rev. D **15**, 2929 (1977).
[3] C. G. Callan, Jr. and S. Coleman, The fate of the false vacuum. 2. First quantum corrections, Phys. Rev. D **16**, 1762 (1977).
[4] E. J. Weinberg, *Classical Solutions in Quantum Field Theory*, Cambridge Monographs on Mathematical Physics (Cambridge University Press, Cambridge, UK, 2012).
[5] K. Lee and E. J. Weinberg, Decay of the true vacuum in curved spacetime, Phys. Rev. D **36**, 1088 (1987).
[6] L. F. Abbott and S. Coleman, The collapse of an anti-de Sitter bubble, Nucl. Phys. **B259**, 170 (1985).
[7] L. F. Abbott and Q.-H. Park, Gravitational stabilization of scalar potentials, Phys. Lett. B **156**, 373 (1985).
[8] Q.-H. Park and L. F. Abbott, Stability and instability of scalar fields coupled to gravity, Phys. Lett. B **171**, 223 (1986).
[9] S. J. Parke, Gravity, the decay of the false vacuum and the new inflationary universe scenario, Phys. Lett. B **121**, 313 (1983).
[10] R. Bousso, B. Freivogel, and M. Lippert, Probabilities in the landscape: The decay of nearly flat space, Phys. Rev. D **74**, 046008 (2006).
[11] A. Aguirre, T. Banks, and M. Johnson, Regulating eternal inflation. II. The great divide, J. High Energy Phys. 08 (2006) 065.
[12] D. A. Samuel and W. A. Hiscock, Effect of gravity on false vacuum decay rates for O(4) symmetric bubble nucleation, Phys. Rev. D **44**, 3052 (1991).
[13] T. Banks, Heretics of the false vacuum: Gravitational effects on and of vacuum decay. 2., arXiv:hep-th/0211160.
[14] T. Banks and J. F. Fortin, Tunneling constraints on effective theories of stable de Sitter space, Phys. Rev. D **80**, 075002 (2009).
[15] S. Kanno and J. Soda, Exact Coleman-De Luccia instantons, Int. J. Mod. Phys. D **21**, 1250040 (2012).
[16] S. Kanno, M. Sasaki, and J. Soda, Tunneling without barriers with gravity, Classical Quantum Gravity **29**, 075010 (2012).
[17] B.-H. Lee, W. Lee, D. Ro, and D. Yeom, Instantons near a tachyonic top in an anti-de Sitter and the no-boundary regulator, Classical Quantum Gravity **32**, 165013 (2015).
[18] J. R. Espinosa, J. F. Fortin, and M. Trépanier, Consistency of scalar potentials from quantum de Sitter space, arXiv:1508.05343.
[19] V. Branchina, E. Messina, and D. Zappala, Impact of gravity on vacuum stability, arXiv:1601.06963.
[20] S. Weinberg, Does Gravitation Resolve the Ambiguity among Supersymmetry Vacua?, Phys. Rev. Lett. **48**, 1776 (1982).
[21] A. Ceresole, G. Dall'Agata, A. Giryavets, R. Kallosh, and A. D. Linde, Domain walls, near-BPS bubbles, and probabilities in the landscape, Phys. Rev. D **74**, 086010 (2006).
[22] M. Dine, G. Festuccia, A. Morisse, and K. van den Broek, Metastable domains of the landscape, J. High Energy Phys. 06 (2008) 014.
[23] M. Dine, G. Festuccia, and A. Morisse, The fate of nearly supersymmetric vacua, J. High Energy Phys. 09 (2009) 013.
[24] G. W. Gibbons and S. W. Hawking, Action integrals and partition functions in quantum gravity, Phys. Rev. D **15**, 2752 (1977).
[25] S. Coleman, V. Glaser, and A. Martin, Action minima among solutions to a class of Euclidean scalar field equations, Commun. Math. Phys. **58**, 211 (1978).